Air-cooled gas-turbine discs: a review of recent research

J. M. Owen
Thermo-Fluid Mechanics Research Centre, School of Engineering & Applied Sciences, University of Sussex, Falmer, Brighton, Sussex, UK

Accepted for publication August 1988

The flow between corotating compressor or turbine discs and the flow between a turbine disc and an adjacent stationary casing can be respectively modelled by a rotating cavity and by a rotor-stator system. This paper reviews some of the recent experimental and theoretical work on flow and heat transfer in these two classes of rotating-disc systems. Comparisons between the theoretical and measured distributions of velocity, pressure, and Nusselt numbers are made for the rotating cavity with a superimposed radial flow of cooling air. For the rotor-stator system, some recent work on the fluid dynamics is outlined, and particular mention is made of the so-called "ingress problem" and of the use of pre-swirl air to improve the blade-cooling effectiveness.

Keywords: rotating discs; gas turbines; fluid dynamics

Introduction

In modern industrial gas turbines and aero-engines, a small percentage of the compressed air is bled off for cooling and sealing purposes. Some of the air is used for cooling the turbine blades and nozzle guide vanes, and part of it is employed in cooling and sealing the turbine discs. It is the latter application that is the subject of this paper.

Figure 1 shows simplified diagrams of disc-cooling systems that are commonly used. In Figure 1(a), a turbine disc rotates close to a stationary casing, and a radial outflow of air is used both to cool the disc and to stop the ingress of hot mainstream gas past the seals into the wheel-space. The turbine designer needs to be able to calculate the temperature of the disc in order to predict its stress, growth and life. The designer wants to know how much air is necessary to seal the system and what the effect is of this air flow on heat transfer rates, frictional windage and pressure distributions.

In many applications, the blade-cooling air is supplied through pre-swirl nozzles in the stationary casing. These nozzles swirl the flow in the direction of the disc rotation so that the temperature of the cooling air relative to the blades is reduced. The designer needs to know the effectiveness of this pre-swirl system and how it affects rim seals, and he should be able to estimate the degree of mixing or "contamination" between the pre-swirl flow and the disc-cooling air.

Figure 1(b) shows a simplified diagram of the cooling flow between corotating turbine discs where air is fed into the system near the center and leaves through holes in an outer shroud. Again, the designer wishes to predict the heat transfer rates, the frictional windage and pressure distributions. The latter is of particular importance in the compressor stages where the cooling air is sometimes extracted between two corotating compressor discs. There is a tendency for free-vortex flow to develop as the air flows radially inward, and the resulting pressure drop can cause a significant reduction in the amount of coolant that can be bled off.

In order to understand the above flows, it is convenient to divide them into two categories: rotor-stator systems, as shown in Figure 1(a), and rotating cavities, as shown in Figure 1(b). It is simpler to consider plane geometries first, after which the effect of practical geometries can be examined. Such rotating-disc research has been carried out over a number of years at the Thermo-Fluid Mechanics Research Centre (TFMRC), University of Sussex, UK, where recent work has concentrated on the problems that are of particular interest to the designer. A review of this work is presented below.

In the following sections, the basic equations and some relevant solutions are presented, followed by a discussion of the rotating-cavity and rotor-stator systems.

The basic equations

The boundary-layer equations

Many, although by no means all, of the problems of practical importance can be described by the boundary-layer equations. For incompressible axisymmetric flow in a stationary polar-coordinate system, the time-average continuity, momentum and energy equations can be written as

$$\frac{\partial V_r}{\partial r}+\frac{V_r}{r}+\frac{\partial V_z}{\partial z}=0 \tag{1}$$

$$V_r\frac{\partial V_r}{\partial r}+V_z\frac{\partial V_r}{\partial z}-\frac{V_\phi^2}{r}=-\frac{1}{\rho}\frac{\mathrm{d}p}{\mathrm{d}r}+\frac{1}{\rho}\frac{\partial \tau_r}{\partial z} \tag{2}$$

$$V_r\frac{\partial V_\phi}{\partial r}+V_z\frac{\partial V_\phi}{\partial z}+\frac{V_rV_\phi}{r}=\frac{1}{\rho}\frac{\partial \tau_\phi}{\partial z} \tag{3}$$

$$V_r\frac{\partial T}{\partial r}+V_z\frac{\partial T}{\partial z}=-\frac{1}{\rho c_p}\frac{\partial q}{\partial z}+\frac{1}{\rho c_p}\mu\Phi \tag{4}$$

$$\tau_r=\mu\frac{\partial V_r}{\partial z}-\overline{\rho V_r'V_r'} \tag{5}$$

$$\tau_\phi=\mu\frac{\partial V_\phi}{\partial z}-\overline{\rho V_\phi'V_z'} \tag{6}$$

$$q=-\left(k\frac{\partial T}{\partial z}-\rho C_p\overline{T'V_z'}\right) \tag{7}$$

$$\mu\Phi=\tau_r\frac{\partial V_r}{\partial z}+\tau_\phi\frac{\partial V_\phi}{\partial z} \tag{8}$$

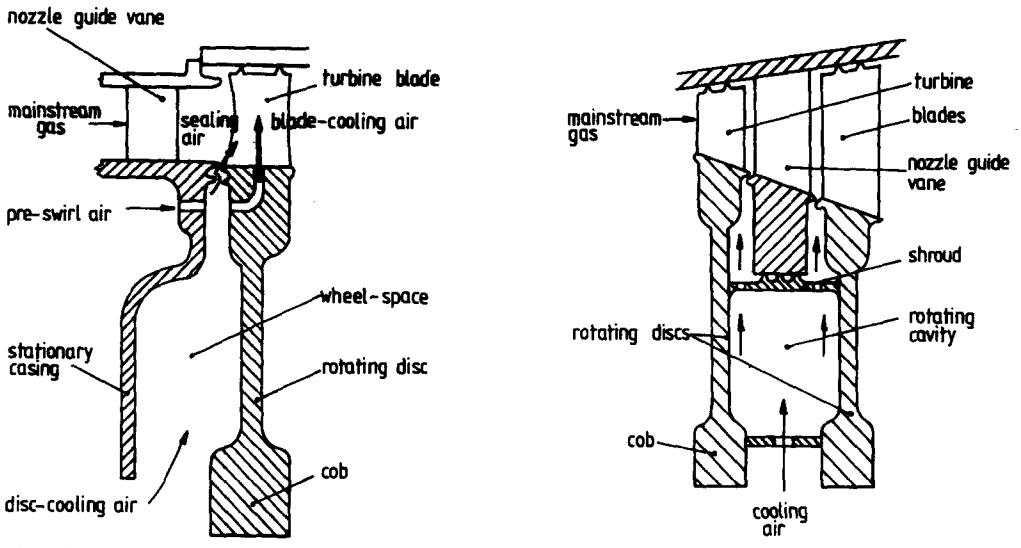

(a) Cooling flows between a turbine disc and a stationary casing.

(b) Cooling flow between corotating turbine discs.

Figure 1 Simplified representation of air-cooled gas-turbine discs

Notation

a, b	Inner, outer radius of disc
A, B	Constants
$C\ (=V_\phi/\Omega r)$ at $r=b$)	Inlet swirl-fraction
$C_m\ (=M/\frac{1}{2}\rho\Omega^2 b^5)$	Moment coefficient
c_p	Specific heat at constant pressure
$C_P\ (=(p_b-p_a)/\frac{1}{2}\rho\Omega^2 b^2)$	Pressure coefficient
$C_w\ (=Q/vb)$	Nondimensional flow rate
$D\ (=(\nu/\Omega)^{1/2})$	Ekman layer thickness
$G\ (=s/b)$	Gap ratio
$G_c\ (=s_c/b)$	Shroud-clearance ratio
h	Axial height of fin
k	Thermal conductivity of fluid
K	Constant
M	Frictional moment on one side of disc
n	Number of fins on disc
$\mathrm{Nu}\ (=q_s r/k(T_s-T_I))$	Local Nusselt number
p	Pressure
$P_{\max}\ (=\rho\Delta p_{\max} b^2/\mu^2)$	Nondimensional pressure asymmetry
Pr	Prandtl number
q_s	Heat flux from disc to cooling air
Q	Volumetric flow rate
r	Radial coordinate
R	Recovery factor
$\mathrm{Re}_r\ (=\lvert Q\rvert/2\pi\nu r)$	Radial Reynolds number
$\mathrm{Re}_\phi\ (=\Omega b^2/\nu)$	Rotational Reynolds number
s	Axial clearance between one disc and the other disc or stator
s_c	Shroud clearance
S_r	Swirl ratio
T	Temperature
u, v, w	Radial, tangential, axial component of velocity in a rotating frame
V_r, V_ϕ, V_z	Radial, tangential, axial component of velocity in a stationary frame
$x\ (=r/b)$	Nondimensional radius
z	Axial distance from disc
$\beta\ (=V_{\phi,c}/\Omega r)$	Relative rotation of core
δ	Boundary-layer thickness
$\Delta p_{\max}$	Maximum circumferential pressure difference in annulus
$\Delta T\ (=C_p(T_p-T_b)/\frac{1}{2}\Omega^2 r_b^2)$	Nondimensional temperature difference
$\eta\ (=z/\delta)$	Nondimensional boundary-layer thickness
$\lambda_L\ (=C_w\,\mathrm{Re}_\phi^{-1/2})$	Laminar-flow parameter
$\lambda_T\ (=C_w\,\mathrm{Re}_\phi^{-4/5})$	Turbulent-flow parameter
μ	Absolute viscosity
$\nu\ (=\mu/\rho)$	Kinematic viscosity
ρ	Density
τ_r, τ_ϕ	Radial, tangential component of shear stress
$\chi=\left(\frac{4b}{\mathrm{Knh}}\frac{\lvert C_w\rvert}{\mathrm{Re}_\phi}\right)^{1/2}$	Nondimensional flow parameter
Ω	Angular speed of disc

Subscripts

a	Refers to conditions at $r=a$
b	Refers to conditions at $r=b$ or refers to blade-cooling air
c	Refers to conditions in core
d	Refers to disc-cooling air
e	Edge of source region
f	Inner edge of fins
I	Refers to conditions at inlet
ℓ	Local value
min	Minimum value
p	Refers to pre-swirl air
s	Refers to conditions at surface of disc
*	Refers to conditions for $C_w=0$

The overbars, which signify time-average values of the fluctuating components, are used only for the turbulent flux terms. In laminar flow these fluctuating components are identically zero.

If separate boundary layers exist on the two discs (one of which rotates and the other is either rotating or stationary), then the radial pressure gradient can be determined from

$$\frac{1}{\rho}\frac{dp}{dr}=\frac{V_{\phi,c}^2}{r} \tag{9}$$

where the subscript c refers to conditions in the rotating core of fluid between the boundary layers.

The above system of partial differential equations can be solved numerically. Alternatively, they can be converted to integral equations, and the resulting ordinary differential equations can then be solved analytically or numerically.

If the boundary-layer equations are expressed in a rotating coordinate system then it is often possible to obtain a simpler linear form referred to as the Ekman-layer equations.

The Ekman layer equations

These equations were first derived by Ekman[1] in connection with flow in the ocean. If Equations 2 and 3 are expressed in a coordinate system rotating at the same angular speed Ω as the rotating disc, and if the nonlinear inertial terms are sufficiently small (which can be shown to be the case when the relative speed difference between the fluid core and the disc is small), it follows that Coriolis terms dominate and

$$-2\Omega(v-v_c)=\frac{1}{\rho}\frac{\partial \tau_r}{\partial z} \tag{10}$$

$$2\Omega u=\frac{1}{\rho}\frac{\partial \tau_\phi}{\partial z} \tag{11}$$

where $u=V_r$ and $v=V_\phi-\Omega r$ are the components of velocity referred to the rotating disc. The appropriate boundary conditions are

$$\begin{aligned} &u=v=0 \text{ at } z=0\\ &u=0,\ v=v_c \text{ as } z\to\infty \end{aligned} \tag{12}$$

The resulting boundary layers are usually referred to as Ekman layers.

Exact solutions for laminar flow

For laminar flow, where the fluctuating terms in Equations 5 and 6 are zero, Equations 10–12 can be solved to give

$$u=-v_c e^{-z/D}\sin z/D \tag{13}$$

and

$$v=v_c(1-e^{-z/D}\cos z/D) \tag{14}$$

where

$$D=(\nu/\Omega)^{1/2} \tag{15}$$

The local volumetric flow rate, Q_ℓ, in the Ekman layer can be found from

$$Q_\ell=2\pi r\int_0^\infty u\,dz \tag{16}$$

Hence, using Equation 13,

$$\frac{Q_\ell}{\nu b}=-\pi\,\mathrm{Re}_\phi^{1/2}\frac{v_c}{\Omega r}x^2 \tag{17}$$

Equation 17 can be used in either of two ways: if Q_ℓ is known, v_c can be found; if v_c is known, Q_ℓ can be determined. It should be noted that if v_c is positive (that is, if the core rotates faster than the disc) then Q_ℓ is negative and the fluid flows radially inward; the converse is also true.

Approximate solutions for turbulent flow

For turbulent flow, if the 1/7th power-law profiles are used then

$$\begin{aligned} &u=u_1\eta^{1/7}(1-\eta),\quad n\leqslant 1\\ &u=0,\quad \eta>1\\ &v=v_c\eta^{1/7},\quad \eta\leqslant 1\\ &v=v_c,\quad \eta>1 \end{aligned} \tag{18}$$

where $u_1=u_1(r)$ and $\eta=z/\delta$, δ being the Ekman layer thickness. The shear stresses are given by the Blasius relationships

$$\frac{\tau_{r,s}}{\rho}=\frac{u_1}{v_c}\frac{\tau_{\phi,s}}{\rho}=0.0225\left(\frac{\nu}{\delta}\right)^{1/4}u_1(u_1^2+v_c^2)^{3/2} \tag{19}$$

where the subscript s refers to the surface of the disc at $z=0$.

Integration of Equations 10 and 11 from $z=0$ to ∞ given

$$\begin{aligned} &\frac{\tau_{r,s}}{\rho}=-\tfrac{1}{4}\Omega v_c\delta\\ &\text{and}\\ &\frac{\tau_{\phi,s}}{\rho}=-\tfrac{49}{60}\Omega u_1\delta \end{aligned} \tag{20}$$

Hence $u_1/v_c=-0.553$,

$$\frac{\delta}{b}=0.0983\,\mathrm{Re}_\phi^{1/5}\left|\frac{v_c}{\Omega r}\right|^{3/5}x^{3/5} \tag{21}$$

and

$$\frac{Q_\ell}{\nu b}=-(\operatorname{sgn} v_c)0.140\,\mathrm{Re}_\phi^{4/5}\left|\frac{v_c}{\Omega r}\right|^{8/5}x^{13/5} \tag{22}$$

As for the laminar case, the flow is radially inward if v_c is positive, and Equation 22 can be used to determine either Q_ℓ or v_c.

The rotating cavity with source-sink flow

The flow structure

The flow structure inside rotating cavities with a radial inflow ($C_w<0$) or outflow ($C_w>0$) of fluid, see Figure 2, has been studied in Refs. 2–5. For radial outflow, the flow is assumed to enter the cavity uniformly at $r=a$ and to leave through a central slot or a series of holes in the shroud at $r=b$. The incoming flow forms a source region near the center, where fluid is entrained into the boundary layers on each disc. After all the fluid has been entrained, Ekman layers form on the discs, and the core of fluid between them rotates at the speed necessary to prevent further entrainment. (Strictly, the term Ekman layer is applied to boundary layers in which the nonlinear terms are negligible. However, it is used here for the nonentraining boundary layers outside the source region, even if the nonlinear terms are not negligible.) For an isothermal or a symmetrically heated cavity, the flow rate is the same in each Ekman layer, and there are no radial or axial components

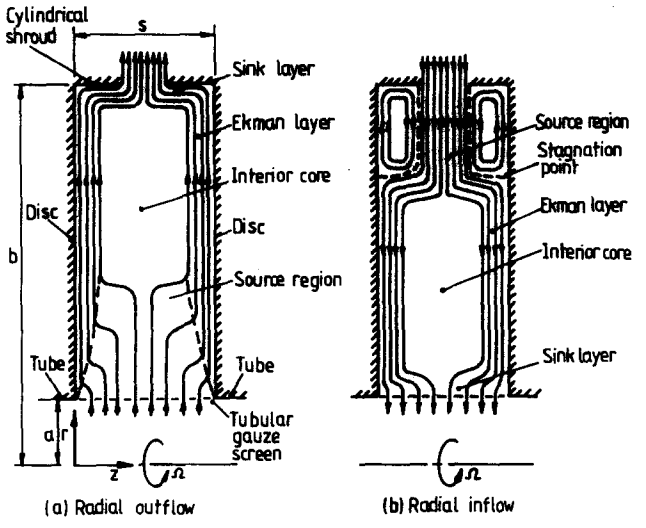

Figure 2 Schematic diagram of source-sink flow in a rotating cavity

of velocity in the core. The sink layer transfers the fluid from the Ekman layers to the outlet in the shroud.

For radial inflow (see Figure 2(b)) the structure is similar but the source region and sink layers form near the shroud and the center of the cavity, respectively. In the source region, outside the boundary layers on the discs, viscous effects are negligible and the angular momentum of the incoming fluid is conserved such that $rV_{\phi,c}=$constant. Consequently, if $V_{\phi,c}<\Omega b$ at $r=b$, there will be a radius r' say, where $V_{\phi,c}=\Omega r'$. Hence, $V_{\phi,c}<\Omega r$ for $r'<r<b$, and the flow in the boundary layers in this region of the discs will be radially outward; for $r<r'$, where $V_{\phi,c}>\Omega r$, this flow in the boundary layers will be radially inward. This creates the recirculation in the source region shown in Figure 2(b).

The size of the source region can be estimated by assuming that it extends to the radius where all the available fluid has been entrained. For radial outflow, using the results given in Equations 17 and 22, this technique gives

$$x_e=A\lambda_L^{1/2} \tag{23}$$

for laminar flow and

$$x_e=B\lambda_T^{5/13} \tag{24}$$

for turbulent flow, where x_e is the nondimensional radius of the source region. For a uniform source, Owen, *et al.*[3] gave $A=0.424$ and $B=1.37$; for an axial inlet, where the flow enters through the center of one disc and impinges on the other, the values for the downstream disc are $A=0.599$ and $B=1.79$. For radial inflow, the corresponding expressions are

$$x_e=\left(C-\frac{1}{2\pi}|\lambda_L|\right)^{1/2} \tag{25}$$

for laminar flow, and

$$x_e=(C-2.22|\lambda_T|^{5/8}x_e^{3/8})^{1/2} \tag{26}$$

for turbulent flow, where $C=(V_{\phi,c}/\Omega r)$ at $r=b$.

Figure 3 shows the flow structure with a uniform laminar radial outflow for $a/b=0.1$, $C_w=79$ and $\mathrm{Re}_\phi=2.5\times10^4$ ($\lambda_L=0.500$) according to Chew, *et al.*[6] The photograph was taken using slit illumination of the $r-z$ plane with micro-sized oil particles injected into the air flow. The computation was carried out using an elliptic solver to solve the Navier-Stokes equations. It can be seen that the flow resembles that shown in Figure 2(a), and Equation 23 gives $x_e=0.300$ which is in good agreement with the actual size of the source region.

Figure 4 shows a comparison of the flow structure observed by Farthing and Owen[7] in cavities either with plane discs or with "cobs" (see Figure 1) attached to the center of the discs. The flow enters axially through the center of the left-hand disc and, for $C_w=1760$ and $\mathrm{Re}_\phi=3\times10^5$ ($\lambda_T=0.0731$), the flow is turbulent throughout the cavity. It can be seen that the flow structure is not significantly affected by the cobs, and Equation 24 with $B=1.79$ gives $x_e=0.654$, which is a good approximation of the size of the source region.

For radial inflow, the size of the source region determined by Firouzian, *et al.*[4] was found to be in agreement with Equations 25 and 26.

Velocity distributions

Pincombe[8] measured the radial and tangential components of velocity inside a number of rotating-disc rigs using laser-doppler anemometry (LDA). Predictions of the velocity profiles have been made by Chew, *et al.*,[6] Chew[9] and Morse[10] using elliptic-solvers, by Owen, *et al.*[3] and Firouzian, *et al.*[5] using momentum-integral techniques, and by Ong and Owen[11] using numerical solutions of the boundary-layer equations.

Outside the source region, where nonentraining Ekman layers are formed on the discs, the local volumetric flow rate in each layer is $Q_\ell=\frac{1}{2}Q$. Equations 17 and 22 can then be used to calculate the tangential component of velocity in the core such that

$$\frac{V_{\phi,c}}{\Omega r}=1-\frac{1}{2\pi}\lambda_L x^{-2} \tag{27}$$

for laminar flow, and

$$\frac{V_{\phi,c}}{\Omega r}=1-\mathrm{sgn}(C_w)2.22|\lambda_T|^{5/8}x^{-13/8} \tag{28}$$

for turbulent flow. By equating (27) and (28) it follows that the laminar and turbulent velocities are equal when $\mathrm{Re}_r=180$, which provides a convenient criterion for the transition from laminar to turbulent flow in an Ekman layer.

Figure 5 shows the variation of $V_{\phi,c}/\Omega r$ with C_w for radial outflow according to Owen, *et al.*[3] The curves of the linear theory correspond to Equations 27 and 28, and the nonlinear theory is the numerical solution of the full momentum-integral equations. The agreement between the nonlinear theory and the experimental data is generally very good, and the linear theory provides a good approximation except at the small values of $V_{\phi,c}/\Omega r$. It can also be seen that transition from laminar to turbulent flow does indeed occur at $\mathrm{Re}_r\simeq180$.

Figure 6 shows the axial variation of the radial component of velocity for radial outflow. The laminar linear solution corresponds to Equation 13 and the turbulent linear and nonlinear solutions correspond to the numerical solutions of the turbulent Ekman layer and boundary-layer equations, respectively, according to Ong and Owen; the data were obtained by Pincombe. The nonlinear turbulent curves, which were based on a mixing-length model of turbulence, are in generally good agreement with the data and show the thickening of the boundary layer with increasing C_w.

Morse obtained numerical solutions of the elliptic equations for both radial outflow and inflow using a low-Reynolds-number k-ε turbulence model. Figure 7 shows a comparison between the computed and measured values for the radial-inflow case for both laminar ($C_w=-309$) and turbulent ($C_w=-946$) flow. The swirl fraction C was taken to be 0.59

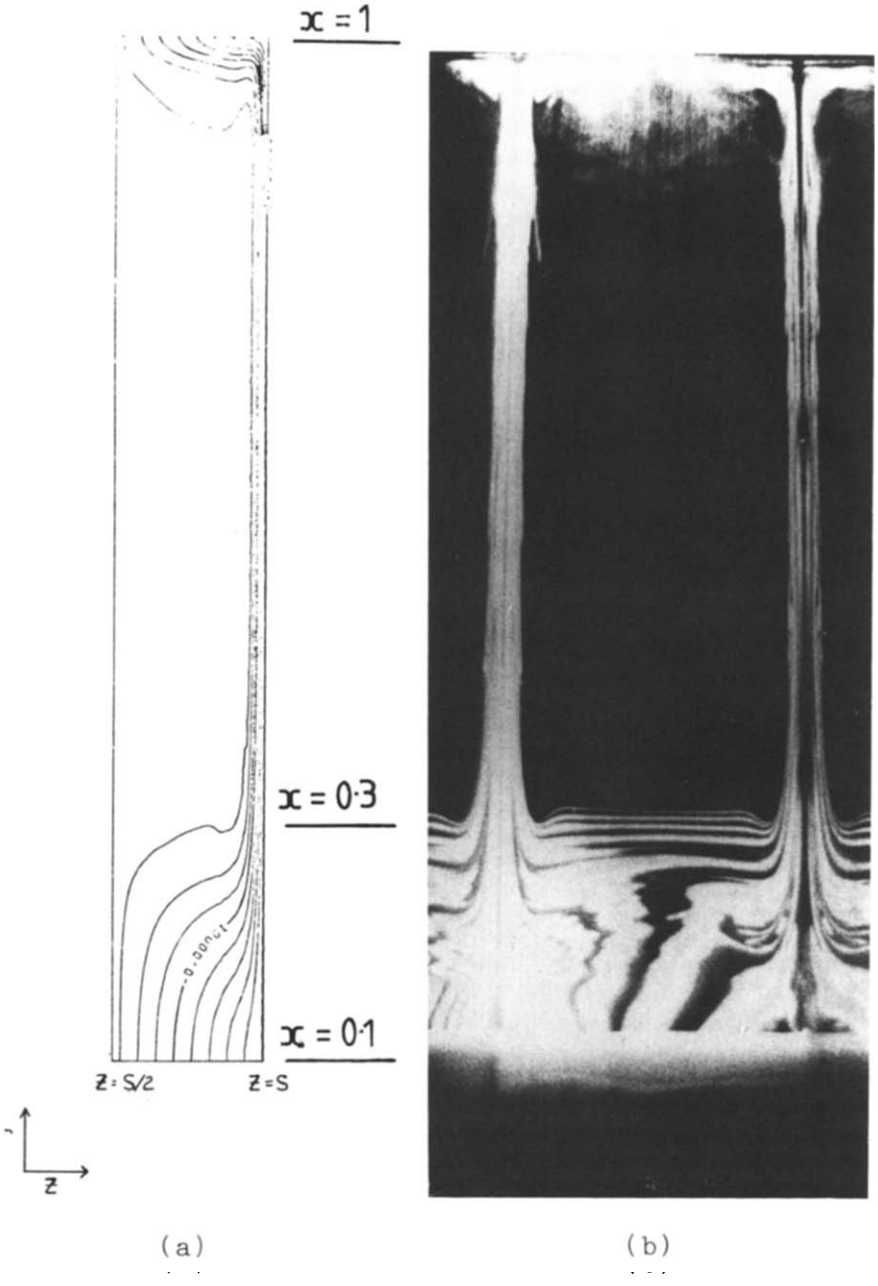

Figure 3 Flow structure for a rotating cavity with a laminar outflow for $Re_\phi = 2.5 \times 10^6$ and $C_w = 79$ (Ref. 6): (a) computed streamlines in the $r-z$ plane for the half-cavity $\frac{1}{2}s \leqslant z \leqslant s$, (b) photographed smoke patterns

for all cases, and it can be seen that the agreement between the computed values and the experimental data is very good.

Pressure distribution for the radial-inflow case

In a gas-turbine engine, if the cooling air is extracted radially inward between two corotating compressor discs, the resulting radial pressure drop can approach that of a free vortex. This may result in the actual flow rate extracted between the discs being less than that required for turbine cooling!

Firouzian, *et al.*[5] obtained a simple expression for the pressure distribution inside a rotating cavity using the results from the linear Ekman layer equations presented above. The pressure gradient was calculated from

$$\frac{1}{\rho}\frac{dp}{dr} = \frac{V_{\phi,c}^2}{r} \tag{29}$$

where in the source region, for $x > x_e$, a free vortex was assumed (such that $V_{\phi,c}/\Omega r = Cx^{-2}$), and for $x < x_e$ Equations 27 and 28 were used for laminar and turbulent flow, respectively. From these results the pressure coefficient C_P can be calculated from

$$C_P = C^2 \int_{x_a}^{1} x(V_\phi/\Omega r)^2 dx \tag{30}$$

$$= (x_e^2 - x_a^2) + 23.7|\lambda_T|^{5/8}(x_e^{3/8} - x_a^{3/8}) + 7.89|\lambda_T|^{5/4}(x_a^{-5/4} - x_e^{-5/4}) + C^2(x_e^{-2} - 1) \tag{31}$$

for turbulent flow, where x_e is given by Equation 26.

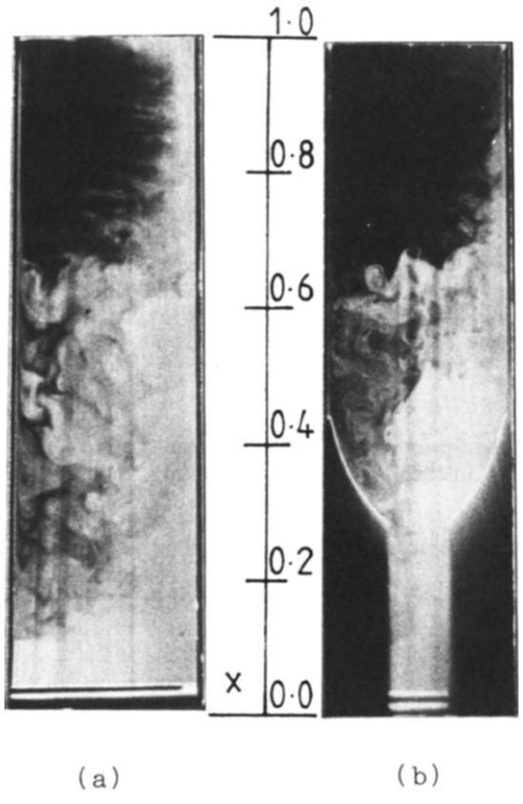

Figure 4 Flow structure in a rotating cavity with a turbulent outflow for $Re_\phi = 3 \times 10^5$ and $C_w = 1760$ (Ref. 7): (a) plane-disc case, (b) disc with cobs

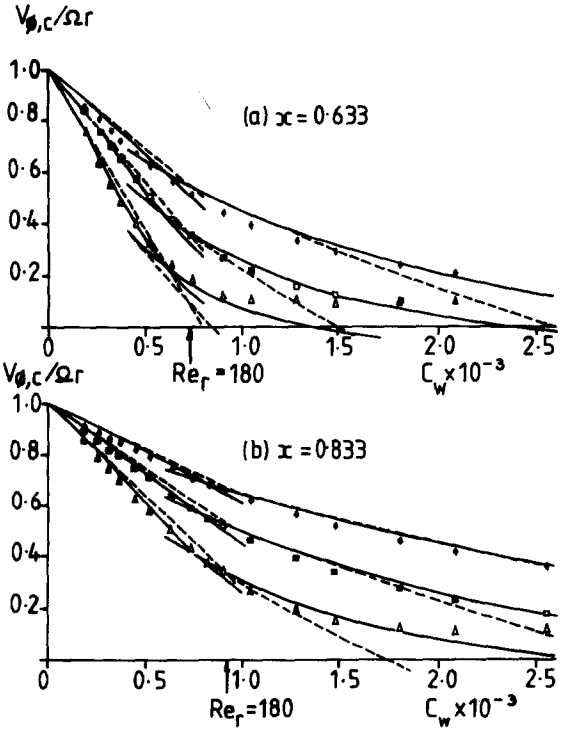

Figure 5 The variation of $V_{\phi,c}/\Omega r$ with C_w for a rotating cavity with a radial outflow. --- linear theory; —— nonlinear theory. Experimental data: ▲ $Re_\phi = 10^5$; ■ $Re_\phi = 2 \times 10^5$; ◆ $Re_\phi = 4 \times 10^5$. Hollow symbols are in the source region (Ref. 3)

Figure 8 shows a comparison between Equation 31, with $C = 0.59$ and $x_a = 0.1$, and the measurements of Firouzian, *et al.* As the measured pressure drops included "inlet" and "exit" losses through the porous shroud and from the center of the rig, the results were corrected using an approximate empirical correlation. Considering the experimental uncertainty and the assumptions made in the theory, the agreement is reasonable. It should be noted that pressure drops over thirty times those

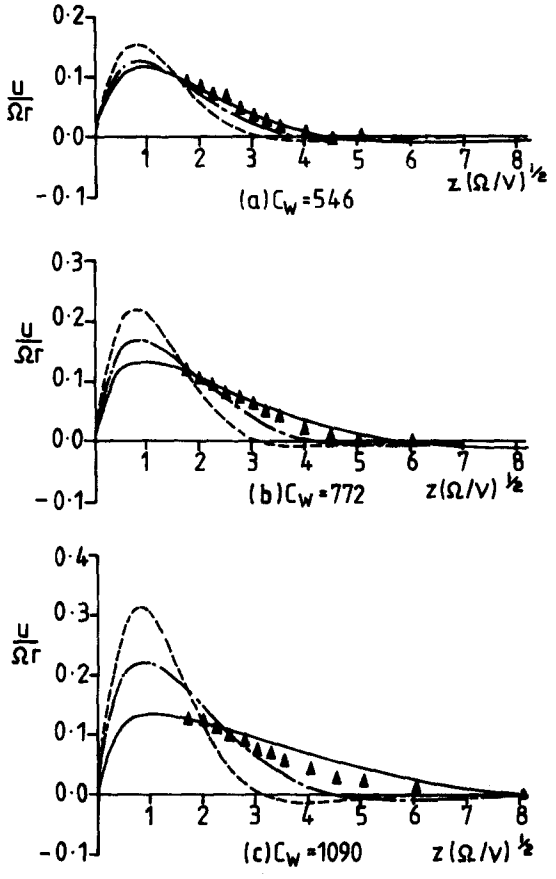

Figure 6 The axial variation of the radial component of velocity for a rotating cavity with a radial outflow for $Re_\phi = 2 \times 10^5$ and $x = 0.633$. —— nonlinear turbulent solution; ——— linear turbulent solution; --- linear laminar solution (Ref. 11), Experimental data (Ref. 8): ▲

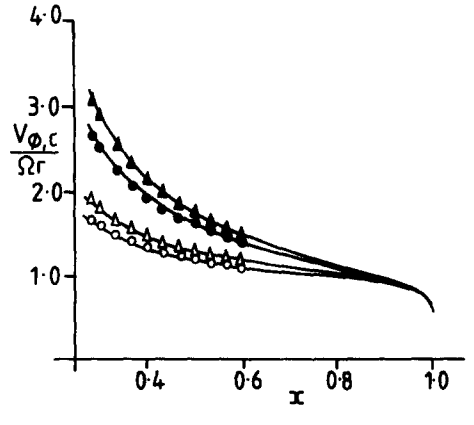

Figure 7 The radial variation of $V_{\phi,c}/\Omega r$ for a rotating cavity with a radial inflow. —— numerical solution (Ref. 10). Experimental data (Ref. 8): △ $C_w = -309$, $Re_\phi = 4 \times 10^5$; ○ $C_w = -309$, $Re_\phi = 6 \times 10^5$; ▲ $C_w = -946$, $Re_\phi = 4 \times 10^5$; ● $C_w = -946$, $Re_\phi = 6 \times 10^5$

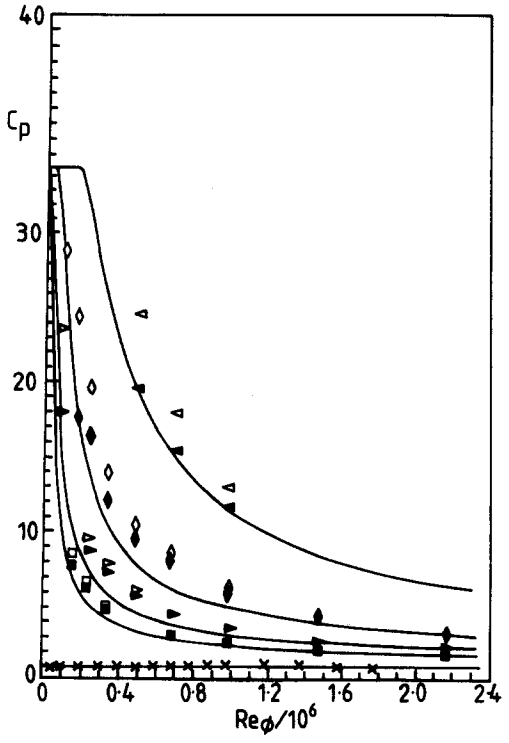

Figure 8 The variation of C_p with Re_ϕ for a rotating cavity with a radial inflow (Ref. 5). —— equation (31) ($C=0.59$, $x_a=0.1$). Experimental data: × $C_w=0$; ■ $C_w=-950$; ▶ $C_w=-1450$; ◆ $C_w=-2750$; ◀ $C_w=-7000$. (Hollow symbols are uncorrected data.)

associated with solid-body rotation were measured and predicted.

Chew and Snell[12] obtained solutions of the momentum-integral equations and predicted the pressure distribution at engine conditions. In addition, Chew, *et al.*[13] carried out a combined theoretical and experimental investigation of the effect of adding radial fins to one of the discs in the rotating cavity. Figure 9 shows a simplified diagram of the experimental rig, where the outer radius of the cavity was $b=381$ mm, and 60 radial fins were attached to one disc from a radius of $r=r_f=168$ mm to $r=b$. The fins had an axial height of $h=10$ mm, and the axial clearance between the edge of the fins and the plane disc was 87 mm. Ten radial vanes, extending axially across the cavity between two central "cobs," were located from the center at $r=a=38$ mm to the start of the fins at $r=r_f$. The vanes ensured that solid-body rotation occurred for $x_a<x<x_f$, where $x_a=a/b=0.1$ and $x_f=r_f/b=0.441$. The holes in the perforated shroud were covered with foam plastic to ensure that the air entered the cavity with solid-body rotation (that is, the swirl fraction, C, was unity).

As well as solving the nonlinear momentum-integral equations, using a rib-roughness model for the resistance of the fins, Chew, *et al.* also obtained a simple solution of the linear Ekman layer equations. The linear theory gives

$$C_p=(x_e^{-2}-1)+(x_e^2-x_a^2)+4\chi(x_e-x_f)+2\chi^2\ln\left(\frac{x_e}{x_f}\right) \qquad (32)$$

where

$$\chi=\left(\frac{4b}{Knh}\frac{|C_w|}{Re_\phi}\right)^{1/2} \qquad (33)$$

and

$$x_e=\tfrac{1}{2}[(\chi^2+4)^{1/2}-\chi] \qquad (34)$$

K, n and h being, respectively, an empirical constant (of order unity), the number, and the axial height of the radial fins.

Figure 10 shows the variation of C_p with $|C_w|/Re_\phi$ for the finned-disc cavity. The "nonlinear theory" indicates solutions of the momentum-integral equations, and the "linear theory" refers to Equation 32. It can be seen that a value of $K=2$ gives a good fit to the experimental data which, like those of Firouzian, *et al.*, were corrected for inlet and exit losses. Without the fins, pressure drops of over thirty times those associated with solid-body rotation were measured.

De-swirl nozzles have been used to reduce the pressure drop in a rotating cavity, and the results of these tests will be reported in the near future.

Heat transfer for the radial-outflow case

Heat-transfer measurements have been made in rigs with a variety of inlet conditions, disc geometries, and radial tempera-

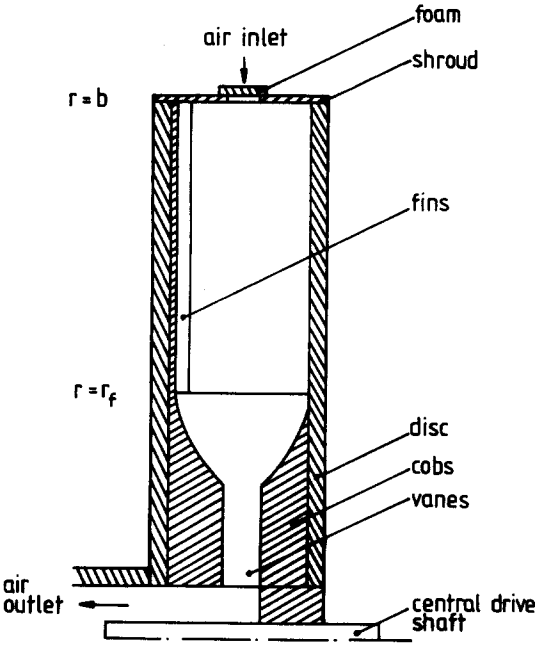

Figure 9 Simplified diagram of the finned-disc rotating-cavity rig

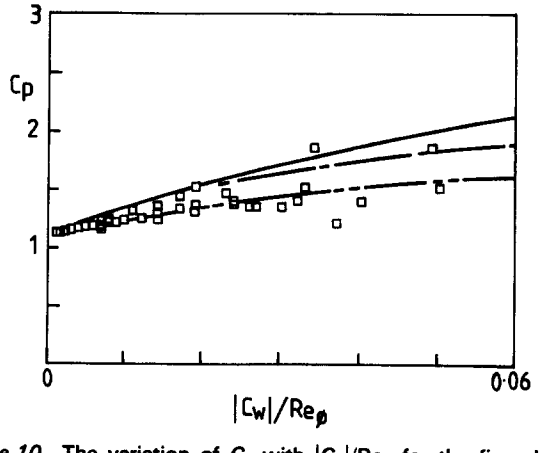

Figure 10 The variation of C_p with $|C_w|/Re_\phi$ for the finned-disc cavity with radial inflow (Ref. 13). —— nonlinear theory; – – – linear theory, $K=1$; – – – – linear theory, $K=2$; □ experimental data

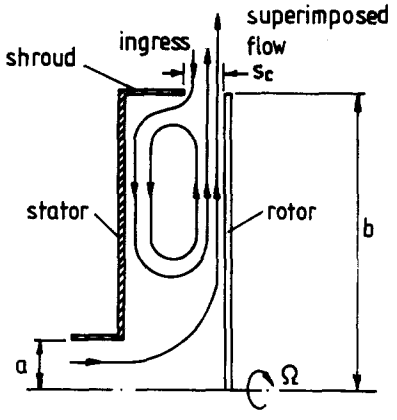

Figure 11 Schematic diagram of a rotor-stator system with radial outflow

ture profiles by Long and Owen[14,15], Farthing and Owen[7] and Northrop and Owen.[16]

In the experiments of Northrop and Owen, the temperature distributions on the discs could be varied by means of built-in electric heaters. The local Nusselt numbers, Nu, were found to depend significantly on the temperature distribution as well as on the coolant flow rate and rotational speed of the cavity. It was also found (for all the heat-transfer measurements referred to above) that the Nusselt number reached a maximum value at a radial location corresponding to the approximate edge of the source region. Inside the source region, where the boundary layers entrain fluid, the Nusselt number increased with radius; outside this region, where nonentraining Ekman layers form, Nu decreased with increasing radius. For the case where the temperature of the disc decreased with increasing radius, the Nusselt numbers could become negative: heat was transferred from the "cooling" air to the disc despite the fact that the temperature of the disc was higher than that of the air entering the cavity.

Predictions of the local Nusselt numbers have been made by Chew and Rogers[17] (using solutions of the integral equations) and by Ong and Owen[18] (using solutions of the differential boundary layer equations). As long as the rotational speed was high enough to ensure that the source region did not fill the entire cavity, the predicted values of Nu were found to be in good agreement with the measurements of Northrop and Owen.

Rotor-stator systems

The basic fluid dynamics

A simplified representation of a rotor-stator system with a superimposed radial outflow of fluid is shown in Figure 11. Fluid enters the system at $r=a$ and leaves at $r=b$ through a clearance between the rotor and the peripheral shroud. At sufficiently high rotational speeds, separate boundary layers form with flow radially outwards on the rotor and inwards on the stator. Between the boundary layer is an inviscid core of rotating fluid in which the radial component of velocity is zero. Ingress occurs when the superimposed flow is unable to prevent external fluid from entering the system through the clearance between the rotor and the shroud.

The isothermal system, without and with a superimposed outflow, has been studied by Daily and Nece[19] and Daily, *et al.*[20] Owen, *et al.*[21] carried out a combined numerical and experimental study of heat transfer in a system with relatively large flow rates. Chew and Vaughan[22] obtained solutions of the elliptic equations using mixing-length models for the turbulent stresses, and their results showed good agreement with the data of Daily, *et al.*

Owen[23] used the Ekman layer equations to obtain approximate solutions for the flow over the rotating and stationary discs. By matching an analytical solution of the turbulent momentum-integral equations for the rotor to the linear Ekman layer solution for the stator, the following expression was obtained for the tangential component of velocity in the core:

$$(1-\beta)^{8/5}(1-0.51\beta)-0.638\beta^{4/5}=4.57\lambda_T x^{-13/5} \tag{35}$$

where $\beta=V_{\phi,c}/\Omega r$. For no superimposed flow, where $\lambda_T=0$, $\beta=\beta^*=0.426$, which is in good agreement with the data of Daily and Nece.

Daily, *et al.* correlated their velocity measurements by

$$\beta/\beta^*=(12.7\lambda_T x^{-13/5}+1)^{-1} \tag{36}$$

and Equations 35 and 36 are shown in Figure 12 together with the computations of Vaughan and the LDA measurements of El-Oun and Pincombe (see Vaughan[24]). Vaughan's computations are in good agreement with the experimental data, and Equation 36 provides a reasonable correlation; Equation 35 tends to underestimate the core rotation at the larger values of λ_T.

For turbulent flow with $\lambda_T<0.219$, Owen's approximate solution gives

$$C_m\,\mathrm{Re}_\phi^{1/5}=0.0729x_e^{23/5}+0.0398\{(1-x_e^{23/5}) +14.7\lambda_T(1-x_e^2)+90.4\lambda_T^2(1-x_e^{-3/5})\} \tag{37}$$

where C_m is the moment coefficient and

$$x_e=1.79\lambda_T^{5/13} \tag{38}$$

For $\lambda_T=0$, $C_m=C_m^*=0.0398\,\mathrm{Re}_\phi^{-1/5}$; for $\lambda_T=0.219$, $C_m=0.0729\,\mathrm{Re}_\phi^{-1/5}$, which is identical to von Karman's[25] solution for a free disc. It should be noted that $\lambda_T=0.219$ implies that

$$C_w=0.219\,\mathrm{Re}_\phi^{4/5} \tag{39}$$

which is equal to the flow rate entrained by a free disc. For $\lambda_T<0.06$, Equation 37 is in good agreement with the computations of Vaughan and with the empirical correlations of Daily, *et al.* For larger values of λ_T, the computations of Chew and Vaughan for a rotor-stator system with a radial inlet show that C_m reaches a constant value, slightly less than the free-disc case,

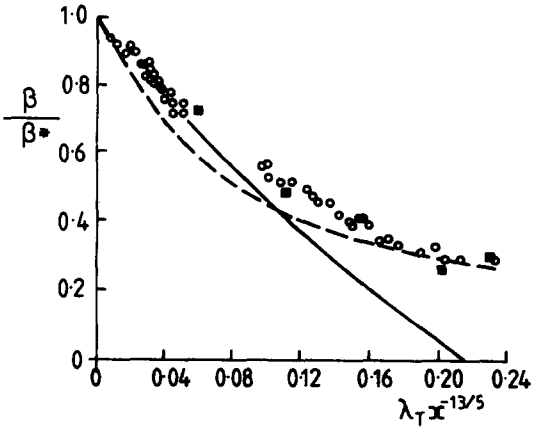

Figure 12 The variation of the relative rotation of the core in a rotor-stator system with radial outflow. —— equation 35; --- equation 36; ○ experimental data of El-Oun and Pincombe; ■ numerical data of Vaughan (Ref. 24)

when $\lambda_T \gtrsim 0.22$; for the axial-inlet case, C_m can exceed the free-disc value.

Sealing rotor-stator systems

As discussed above, in a rotor-stator system the core of fluid between the boundary layers rotates with an angular speed that is attenuated by increasing flow rate. This rotation creates a radal pressure gradient, and the pressure in the "wheel-space" between the two discs increases with radius. If there is a small clearance between the shroud and the rotor, as shown in Figure 11, then some of the fluid in the rotor boundary layer is "pumped" out of the system. When there is no, or little, superimposed flow, the outflow is compensated by an inflow of external fluid, referred to as ingress. As the superimposed flow is increased, the pressure drop across the shroud causes the system to be pressurized, and the ingress can be prevented.

Bayley and Owen[26] studied a system with an axial-clearance seal, as shown in Figure 11, for the case where the axial clearance, S_c, was small. Assuming viscous effects were negligible, they showed the minimum nondimensional flow rate necessary to prevent ingress, $C_{w,\min}$, should be given by

$$C_{w,\min} = K G_c \, \mathrm{Re}_\phi \tag{40}$$

where K is an empirical constant. For $G = 0.06$, 0.12 and 0.18, $G_c = 0.0033$ and 0.0067, and $\mathrm{Re}_\phi \leqslant 4 \times 10^6$, they conducted experiments to determine $C_{w,\min}$ by measuring the pressure drop across the shroud and found that a value of $K = 0.61$ correlated their data.

In a more comprehensive experimental study, Phadke and Owen[27] investigated the sealing characteristics of seven different geometries, including seals with radial clearances. Pressure and gas concentration measurements were made to determine $C_{w,\min}$ for $G = 0.1$, $0.0025 \leqslant G_c \leqslant 0.04$ and $\mathrm{Re}_\phi \leqslant 1.2 \times 10^6$. All three techniques yielded qualitatively similar results, and $C_{w,\min}$ was correlated by an expression of the form

$$C_{w,\min} = K G_c^m \, \mathrm{Re}_\phi^n \tag{41}$$

where K, m and n are empirical constants that depend on the seal and the ingress criterion used.

With axial-clearance seals, the pressure inside the wheel-space decreases with increasing rotational speed. However, with the radial-clearance seals, the pressure could increase with rotational speed. This increase was termed the "pressure-inversion effect" and is believed to be caused by the flow on the rotor impinging on the stationary shroud, or on the stator, thereby forming a curtain of fluid that seals the system. As a consequence, the radial-clearance seals tended to be more effective than the others.

The above tests were all carried out in a rig in which the external fluid was stationary. In an engine, the mainstream gas flows axially across the outside of the seals, and may be swirling and nonaxisymmetric because of the upstream nozzle guide vanes and combustion chambers. Abe, *et al.*[28] obtained results to suggest that, with an external flow of air, the sealing flow rate $C_{w,\min}$ was virtually independent of rotational speed.

A separate series of experiments was carried out by Phadke and Owen[29] for a rotor-stator system with an external flow of air. The rig was surrounded by a stationary cylindrical enclosure which created an annulus and air flowed axially through the annulus, from the stator towards the rotor. It was not possible to achieve perfectly axisymmetric external flow, and it was found that ingress could occur even when the rotor was stationary: fluid moved laterally across the wheel-space from high-pressure to low-pressure regions in the annulus.

At low values of Re_w (the external-flow Reynolds number), $C_{w,\min}$ was proportional to Re_ϕ. At high values of Re_w, $C_{w,\min}$ became independent of Re_ϕ and became proportional to Re_w. This effect is shown in Figure 13 for an axial-clearance seal with $G_c = 0.02$. It is interesting to observe that, for the smaller values of Re_w, $C_{w,\min}$ can actually decrease with increasing Re_w.

The numerical solutions of Vaughan[24] throw light on the sealing behavior illustrated in Figure 13. For computations with $G = 0.1$, $G_c = 0.01$, $C_w = 10^3$, $\mathrm{Re}_\phi = 8 \times 10^5$ and $0 \leqslant \mathrm{Re}_w \leqslant 6 \times 10^5$, the streamlines show that, for axisymmetric flow, fluid ingested into the wheel-space from the external flow tends to separate from the shroud. The resulting separation bubble decreases the effective clearance between the shroud and the rotor, thereby reducing the amount of sealing air required to prevent ingress. The separation bubble grows in size with increasing Re_w suggesting that $C_{w,\min}$ should decrease with increasing Re_w.

Under nonaxisymmetric conditions, external flow can impinge on the rotor at some circumferential locations, and this results in radial inflow at these locations and outflow at others. Thus, for nonaxisymmetric flow, $C_{w,\min}$ increases with increasing Re_w. There is, therefore, a minimum value of $C_{w,\min}$ at the point where the nonaxisymmetric impingement is balanced by the axisymmetric sealing effect of the external flow. Vaughan's potential-flow solutions for the nonaxisymmetric case show that the sealing flow rate is proportional to the external axial velocity, a result that is consistent with the experimental evidence.

For nonaxisymmetric flow, ingress is affected by the circumferential pressure distribution in the external-flow annulus, and Phadke and Owen[30] carried out tests in which the pressure symmetry could be varied independently of Re_w. They were able to show that circumferential pressure differences, rather than Re_w itself, affected $C_{w,\min}$. Using a simple inviscid model, they obtained a correlation for the stationary-disc case expressing $C_{w,\min}$ in terms of $\Delta p_{\max}$, the difference between the maximum and minimum static pressures in the external-flow annulus, such that

$$C_{w,\min} = 2\pi K G_c P_{\max}^{1/2} \tag{42}$$

where K is an empirical constant and

$$P_{\max} = \rho \, \Delta p_{\max} b^2 / \mu^2 \tag{43}$$

A value of $K = 0.6$ was found to correlate most of their data with reasonable accuracy.

Phadke and Owen tentatively suggested that Equation 41, for $\mathrm{Re}_w = 0$, and Equation 43, for $\mathrm{Re}_\phi = 0$, could be used as asymptotes to provide an estimate of $C_{w,\min}$. The larger of the

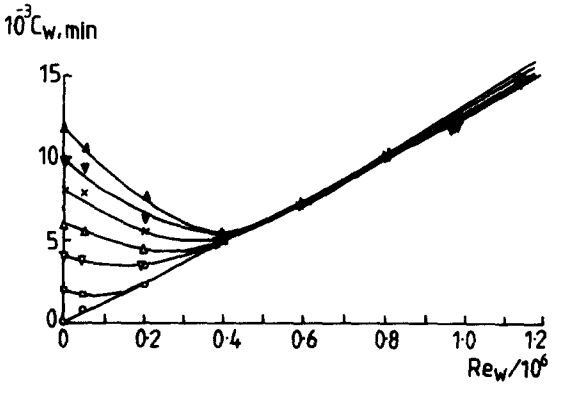

Figure 13 The effect Re_ϕ on the variation of $C_{w,\min}$ with Re_w on a rotor-stator rig (Ref. 29)

Symbol	○	□	▽	△	×	▼	▲
$\mathrm{Re}_\phi/10^6$	0	0.2	0.4	0.6	0.8	1.0	1.2

values of $C_{w,min}$ obtained from these two equations should provide a conservative estimate.

El-Oun, *et al.*[31] made measurements, without external flow, in an isothermal rig that was sealed using both a radial outflow of "disc-cooling" air and pre-swirled "blade-cooling" air (as shown in Figure 1(a)). The disc-cooling air was supplied through a hole in the center of the stator, and the pre-swirl air was introduced through 60 nozzles, inclined at an angle of 20° to the tangential direction, located near the outside of the stator. Air left the system through the clearance between the shroud and rotor and also through a series of 60 holes in the outer part of the rotor; the latter represented the blade-cooling feed-holes in an air-cooled turbine disc.

The authors used flow visualization, pressure and concentration measurements to determine $C_{w,min}$ for $G_c = 0.0072$ and for Re_ϕ up to 1.8×10^6. It was found that the value of $C_{w,min}$ obtained with only disc-cooling air was virtually the same as that with only pre-swirl air: $C_{w,min}$ was independent of where the flow was fed into the system. However, when flow was extracted through the blade-cooling holes in the rotor, $C_{w,min}$ was increased; this increase was attenuated if the disc-cooling and pre-swirl flows were used simultaneously. Gas-concentration measurements also showed that the blade-cooling air could be severely contaminated with the disc coolant, and under some conditions all the disc-cooling air could be entrained into the blade-cooling holes.

Ways of reducing the contamination of blade-cooling air with disc coolant are being investigated, and the results will be published in the future.

Pre-swirl blade-cooling effectiveness

As discussed above, one method of introducing blade-cooling air into a rotor-stator wheel-space is by the use of pre-swirl nozzles in the stator. By swirling the air in the direction of rotation, its temperature relative to the rotor is reduced. As the pre-swirl air can mix with the disc coolant, the problem is further complicated if ingress of hot mainstream gas occurs.

Meierhofer and Franklin[32] determined the effectiveness of a pre-swirl system by measuring the temperature of the air in the nozzles and in the rotating channels that feed the coolant to the turbine blades of an actual engine. They obtained a correlation of the effectiveness as a function of the ratio of disc speed to that of the effective pre-swirl velocity at the rotor plane, the latter being determined from temperature measurements.

El-Oun and Owen[33] developed a simple theoretical model to determine, ΔT, the nondimensional temperature drop between nozzles and the blade holes defined as

$$\Delta T = \frac{c_p(T_p - T_b)}{\frac{1}{2}\Omega^2 r_b^2} \tag{44}$$

where T_p and T_b are the total temperatures of the cooling air referred to the stator and the rotor, respectively, and r_b is the radial location of the blade-cooling holes. Using the Reynolds analogy, they showed that for an adiabatic system without mixing of the pre-swirl and disc-cooling flows

$$\Delta T = S_r^2 - R(1 - S_r)^2 \tag{45}$$

where S_r is the swirl ratio (or ratio of the tangential component of velocity of the pre-swirl flow to the angular speed of the disc at $r = r_b$) and R is the recovery factor, which for air was assumed to be equal to $Pr^{1/3}$. For radial outflow, where mixing occurred between the pre-swirl and disc-cooling flows, the authors used the conservation of angular momentum to calculate the effective swirl ratio, and they used the steady-flow energy equation to estimate the increase of enthalpy of the disc-cooling air due to frictional heating.

The apparatus was essentially the same as that used by El-Oun, *et al.*,[31] which is described above. As the maximum speed of the rotor was 5400 rev/min and the radial location of the blade-cooling holes was 0.19 m, the dynamic temperatures were small. Although the error in the measured temperature difference between the pre-swirl and blade-cooling air was estimated to be less than ± 0.3°C, there could be large relative errors in ΔT at the lower rotational speeds (that is, at the higher values of S_r). Despite this, the agreement between theory and experiment was good, as illustrated in Figure 14 which shows the variation of ΔT with S_r for various values of $C_{w,b}$, $C_{w,d}$ and $C_{w,p}$, the nondimensional blade-cooling, disc-cooling, and pre-swirl flow rates, respectively. For unmixed flows, the theory

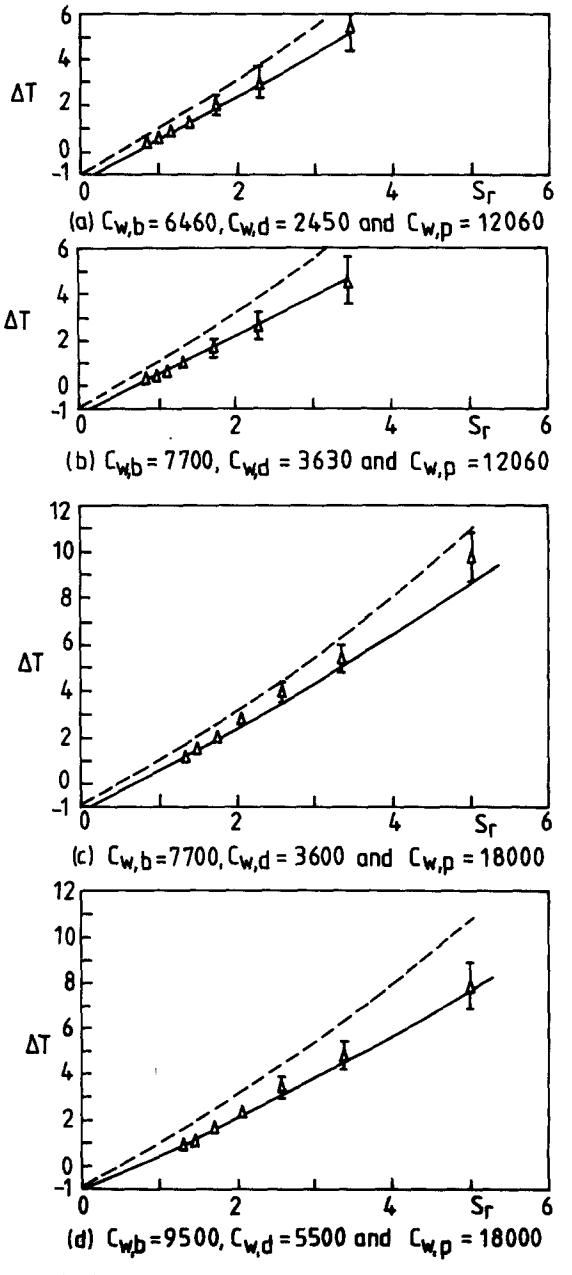

Figure 14 The variation of ΔT with S_r for a rotor-stator rig with pre-swirl and disc-cooling flow (Ref. 33). —— theory for mixed flow; --- theory for unmixed flow; ⊥ experimental data and error bounds

corresponds to Equation 45; for mixed flows, Equation 45 is modified as outlined above. It can be seen that, with few exceptions, the measurements are in very good agreement with the theory for mixed flow.

The authors also conducted experiments in which the disc-cooling air was supplied radially inward from the pre-swirl nozzles. For radial inflow, if $S_r > 1$ then the flow can be radially inward on the rotor as well as on the stator. When this occurs, the frictional moment on the rotor is reversed (that is, power is put into the rotor) and the blade-cooling air is no longer contaminated with disc-coolant. The measured values of ΔT for radial inflow were found to be in good agreement with the unmixed theory, Equation 45.

Concluding remarks

Since the 1984 review given in Ref. 34, considerable progress has been made in understanding the flow and heat transfer that occurs in a variety of rotating-disc systems. The rotating cavity with a radial inflow or outflow of fluid, which is used to model the flow between corotating compressor or turbine discs, is now well understood. Predictions of the flow and heat transfer in rotating cavities are in good agreement with the available experimental data, and it is possible to predict, with reasonable accuracy, the important fluid-dynamic and heat-transfer performance at engine conditions.

The rotor-stator system with a superimposed radial outflow of fluid, which is used to model the flow between a turbine disc and an adjacent stationary casing, has also been extensively studied. The fluid dynamics of these systems can be predicted accurately by both elliptic and boundary-layer equations, but the amount of heat-transfer data relevant to gas-turbine design is still limited. Particular attention has been paid to the 'ingress problem': the determination of the minimum amount of cooling air necessary to prevent the ingestion of hot mainstream gas into the wheel-space of a rotor-stator system. The effect of seal geometry, rotational speed, external flow and pre-swirl flow on the sealing performance has been studied experimentally, but further work is still necessary. In particular, as ingress can be caused by a nonaxisymmetric pressure distribution in the external mainstream flow in a gas turbine, it will be necessary to use three-dimensional elliptic solvers to predict accurately the sealing performance under realistic engine conditions. What happens to ingested hot gas when it enters the wheel-space is also a problem where further work is required.

One case that has not been included in this review is that of the rotating cavity with an axial throughflow of air. This problem occurs when cooling air passes through the centers of hot corotating compressor discs, and some of the air is ingested into the "trapped" cavities between the discs. The ingestion is triggered by vortex breakdown of the central jet of fluid, and the resulting buoyancy-driven flow is three-dimensional and unsteady. It is difficult to obtain reliable data of relevance to the designer, but it is hoped that some results will be published in the near future.

Acknowledgments

I am indebted to those colleagues who conducted much of the research described in this paper and to the Science and Engineering Research Council, Rolls Royce plc, Ruston Gas Turbines plc and Motoren-und Turbinen-Union GmbH, who funded most of the work.

References

1 Ekman, V. W. On the influence of the earth's rotation on ocean currents. *Ark. Mat. Astr. Fys.*, 1905, **2**, 1

2 Owen, J. M. and Pincombe, J. R. Velocity measurements inside a rotating cylindrical cavity with a radial outflow of fluid. *J. Fluid Mech.*, 1980, **99**, 111

3 Owen, J. M., Pincombe, J. R., and Rogers, R. H. Source-sink flow inside a rotating cavity. *J. Fluid Mech.*, 1985, **155**, 233

4 Firouzian, M., Owen, J. M., Pincombe, J. R., and Rogers, R. H. Flow and heat transfer in a rotating cavity with a radial inflow of fluid. Part 1: The flow structure. *Int. J. Heat and Fluid Flow*, 1985, **6**, 226

5 Firouzian, M., Owen, J. M., Pincombe, J. R., and Rogers, R. H. Ibid. Part 2: Velocity, pressure and heat transfer measurements. *Int. J. Heat and Fluid Flow*, 1986, **7**, 21

6 Chew, J. W., Owen, J. M., and Pincombe, J. R. Numerical predictions for laminar source-sink flow in a rotating cylindrical cavity. *J. Fluid Mech.*, 1984, **143**, 451

7 Farthing, P. R. and Owen, J. M. The effect of disc geometry on heat transfer in a rotating cavity with a radial outflow of fluid. *J. Eng. Gas Turbines and Power*, 1988, **110**, 70

8 Pincombe, J. R. Optical measurements of the flow in a rotating cylinder. D.Phil. thesis, University of Sussex, 1983

9 Chew, J. W. Prediction of flow in a rotating cavity with radial outflow using a mixing length turbulence model. *Proc. 4th Int. Conf. on Num. Meth. in Laminar and Turbulent Flow*, Pineridge Press, 1985, 318

10 Morse, A. P. Numerical prediction of turbulent flow in rotating cavities. *32nd ASME International Gas Turbine Conference*, Anaheim. Paper No. 87-GT-74, 1987

11 Ong, C. L. and Owen, J. M. Boundary-layer flows in rotating cavities. *33rd ASME International Gas Turbine Conference*, Amsterdam, Paper No. 88-GT-292, 1988

12 Chew, J. W. and Snell, R. J. Prediction of the pressure distribution for radial inflow between co-rotating discs. *33rd ASME International Gas Turbine Conference*, Amsterdam, Paper No. 88-GT-61, 1988

13 Chew, J. W., Farthing, P. R., Owen, J. M., and Stratford, B. The use of fins to reduce the pressure drop in a rotating cavity with a radial inflow. *33rd ASME International Gas Turbine Conference*, Amsterdam, Paper No. 88-GT-58, 1988

14 Long, C. A. and Owen, J. M. Transient analysis of heat transfer in a rotating cavity with a radial outflow of fluid. *8th Intl. Heat Transfer Conference*, San Francisco, Paper No. JW-18, 1986

15 Long, C. A. and Owen, J. M. The effect of inlet conditions on heat transfer in a rotating cavity with a radial outflow of fluid. *J. Turbomachinery*, 1986, **108**, 145

16 Northrop, A. and Owen, J. M. Heat transfer measurements in rotating-disc systems. Part 2: The rotating cavity with a radial outflow of cooling air. *Int. J. Heat and Fluid Flow*, 1988, **9**, 27

17 Chew, J. W. and Rogers, R. H. An integral method for the calculation of turbulent forced convection in a rotating cavity with radial outflow. *Int. J. Heat and Fluid Flow*, 1988, **9**, 37

18 Ong, C. L. and Owen, J. M. Prediction of heat transfer in a rotating cavity with a radial outflow. Submitted for publication

19 Daily, J. W. and Nece, R. E. Chamber dimension effects on induced flow and frictional resistance of enclosed rotating disks. *J. Basic Engng.*, 1960, **82**, 217

20 Daily, J. W., Ernst, W. D. and Asbedian, V. V. Enclosed rotating disks with superposed throughflow: mean steady and periodic unsteady characteristics of induced flow. Hydrodynamics Lab., Massachusetts Institute of Technology, Report No. 64, 1964

21 Owen, J. M., Haynes C. M., and Bayley, F. J. Heat transfer from an air-cooled rotating disk. *Proc. Roy. Soc. London*, 1974, **A336**, 453

22 Chew, J. W. and Vaughan, C. M. Numerical predictions for the flow induced by an enclosed rotating disc. *33rd ASME International Gas Turbine Conference*, Amsterdam, Paper No. 88-GT-127, 1988

23 Owen, J. M. An approximate solution for the flow between a rotating and a stationary disc. *33rd ASME International Gas Turbine Conference*, Amsterdam, Paper No. 88-GT-293, 1988

24 Vaughan, C. A numerical investigation into the effect of an

external flow field on the sealing of a rotor-stator cavity. D. Phil. thesis, University of Sussex, 1986

25 Karman, Th. von. Über laminare und Turbulente Reibung. *Z. Angew. Math. Mech.*, 1921, **1**, 233

26 Bayley, F. J. and Owen, J. M. The fluid dynamics of a shrouded disc system with a radial outflow of coolant. *J. Engng Power*, 1970, **92**, 335

27 Phadke, U. P. and Owen, J. M. Aerodynamic aspects of the sealing of gas turbine rotor-stator systems. Part 1: The behaviour of simple shrouded rotating-disc systems in a quiescent environment. *Int. J. Heat and Fluid Flow*, 1988, **9**, 98

28 Abe, T., Kikuchi, J. and Takeuchi, H. An investigation of turbine disc cooling (experimental investigation and observation of hot gas flow into a wheelspace). *13th CIMAC Conf.*, Vienna, Paper No. GT-30, 1979

29 Phadke, U. P. and Owen, J. M. Aerodynamic aspects of the sealing of gas turbine rotor-stator systems. Part 2: The performance of simple seals in a quasi-axisymmetric external flow. *Int. J. Heat and Fluid Flow*, 1988, **9**, 106

30 Phadke, U. P. and Owen, J. M. Aerodynamic aspects of the sealing of gas turbine rotor-stator systems. Part 3: The effect of non-axisymmetric external flow on seal performance. *Int. J. Heat and Fluid Flow*, 1988, **9**, 113

31 El-Oun, Z. B., Neller, P. H. and Turner, A. B. Sealing of a shrouded rotor-stator system with pre-swirl coolant. *32nd ASME International Gas Turbine Conference*, Anaheim, Paper No. 87-GT-72, 1987

32 Meierhofer, B. and Franklin, C. J. An investigation of a pre-swirled cooling airflow to a turbine disc by measuring the air temperature in the rotating channels. *26th ASME International Gas Turbine Conference*, Houston. Paper No. 81-GT-132, 1981

33 El-Oun, Z. and Owen, J. M. The effect of superimposed flows on the temperatures in an adiabatic rotor-stator system. *33rd ASME International Gas Turbine Conference*, Amsterdam, Paper No. 88-GT-276, 1988

34 Owen, J. M. Fluid flow and heat transfer in rotating-disc systems. *Heat and mass transfer in rotating machinery*. Eds: Metzger, D. E. and Afgan, N. H. Hemisphere, Washington, 1984